Combustion Synthesis of Nanometric Powders of $LaPO_4$ and Sr-Substituted $LaPO_4$

S. Gallini, J. R. Jurado, and M. T. Colomer*

Instituto de Cerámica y Vidrio, CSIC, C/Kelsen n° 5, Campus de la Universidad Autónoma, 28049 Madrid, Spain

Received November 24, 2004. Revised Manuscript Received March 22, 2005

$La_{(1-x)}Sr_{(x)}PO_4$ materials are very stable at high temperature and water vapor partial pressure and they show protonic conductivity; thus, they could be used as electrolytes in HTPFCs (high-temperature protonic fuel cells), hydrogen sensors, and hydrogen separation technology. This work describes the combustion synthesis of $La_{(1-x)}Sr_{(x)}PO_4$ powders ($x = 0$, 0.025, 0.050) from mixtures of $La(NO_3)_3 \cdot 6H_2O$ and $Sr(NO_3)_2$ as cation precursors, $(NH_4)_2HPO_4$ as anion precursor, and urea as fuel. The characterization of the as-prepared combustion products showed that combustion synthesis provides a straightforward method for the achievement of solid solutions of these materials as nanometric powders. Furthermore, dilatometric studies reveal that dense ceramics can be obtained at low sintering temperature (1300 °C), in air, from the synthesized nanometric powders.

Introduction

Rare-earth phosphates present a high luminescence quantum efficiency and unusual magnetic behavior and, therefore, they find applications in special glasses, laser technology,[1,2] compact fluorescent lamps, and plasma display panels.[3] Phosphates glasses and ceramics are also used in biological implants and glass metal joining.[4] $LaPO_4$ has also been found to be a good oxide interphase material, with a good chemical compatibility with alumina at high temperatures (up to at least 1700 °C).[5−7] Moreover, (La-) monazite crystals, naturally occurring minerals, are known to have survived 10^9 years of weathering; for this reason they are considered as host material for long-term storage of radioactive wastes.[8]

In recent years, the interest in $LaPO_4$ has also focused on its possible application as a high-temperature protonic conductor (HTPC)[9−14] when a small percentage of La is substituted by Sr or Ca. HTPCs are materials in which the conductivity is mainly protonic at temperatures higher than 600 °C. Proton conductivity is the main mechanism in many and diverse processes such as photosynthesis in plants and the production of electricity in electrochemical devices. The interest of the scientific community in Sr:$LaPO_4$ as a proton conductor derives from its high stability at high temperature and high water vapor partial pressure, as mentioned above, a requisite condition for materials applied in high-temperature electrochemical devices.

The authors have demonstrated in a previous article[14] that Sr:$LaPO_4$ prepared by combustion synthesis and sintered at 1300 °C is predominantly a protonic conductor below 700 °C in wet oxygen. In addition, the grain boundary resistance is negligible at 400 °C and higher temperatures and, thus, could be a good candidate as an electrolyte in HTPFCs.

In relation to the preparation of $LaPO_4$, Chen and Mah[15] prepared this material through four different chemical routes. These authors concluded that the two best routes were the direct reaction between La_2O_3 and H_3PO_4 because of the absence of byproducts, and the reaction between the same phosphoric acid with lanthanum hydroxide, although no attempts of doping were made in these cases. According to Lucas et al.,[16] the wet synthesis of rare-earth phosphates by the precipitation method from a rare-earth chloride solution and H_3PO_4 or $(NH_4)_2HPO_4$ always leads to the formation of precipitates crystallized in the hexagonal structure of rhabdophane $RePO_4 \cdot nH_2O$ (Re = La, Ce, or Y). Furthermore, H_3PO_4 adsorbed at the surface of the particles is always present in the precipitates. From these results a unit chemical formula can be proposed as $RePO_4 \cdot nH_2O \cdot (H_3PO_4)x$ with $n \approx 0.5$ for La. The removal of H_3PO_4 is only possible using a high-temperature calcination treatment at 1400 °C in order to achieve its decomposition. Gallini et al.[17] synthesized $La_{(1-x)}Sr_{(x)}PO_4$ powders through coprecipi-

* To whom correspondence should be addressed. E-mail: tcolomer@icv.csic.es.

(1) Danielmeyer, H. G.; Weber, H. P. *J. Quantum Electron.* **1972**, *8*, 805.
(2) Albrand, K. R.; Attig, R.; Fenner, J.; Jesser, J. P.; Moot, D. *Mater. Res. Bull.* **1974**, *9*, 129.
(3) Rao, R. P.; Devine, D. J. *J. Luminescence* **2000**, *87−89*, 1260.
(4) Ohgaki, M.; Kizuki, T.; Katsura, M.; Yamashita, K. *J. Biomed. Mater. Res.* **2001**, *57*, 366.
(5) Morgan, P. E. D.; Marshall, D. B. *Mater. Sci. Eng. A* **1993**, *162*, 15.
(6) Morgan, P. E. D.; Marshall, D. B. *J. Am. Ceram. Soc.* **1995**, *78*, 1553.
(7) Morgan, P. E. D.; Marshall, D. B.; Housley, R. M. *Mater. Sci. Eng. A* **1995**, *195*, 215.
(8) Boatner, L. A.; Beall, G. W.; Abraham, M. M.; Finch, C. B.; Floran, R. J.; Huray, P. G.; Rappaz, M. *The management of Alpha-contaminated wastes*; International Atomic Energy Agency, IAEA-SM-264/73: Vienne, Austria, 1980.
(9) Norby, T.; Christiansen, N. *Solid State Ionics* **1995**, *77*, 240. Amezawa, K.; Kjelstrup, S.; Norby, T.; Ito, Y. *J. Electrochem. Soc.* **1998**, *145*, 10.
(10) Abe, Y.; Hosono, H.; Akita, O.; Hench, L. L. *J. Electrochem. Soc.* **1994**, *141*, 6.
(11) Mellander, B.-E.; Zhu, B.; *Solid State Ionics* **1993**, *61*, 105.
(12) Tyholdt, F.; Horst, J. A.; Jørgensen, S.; Østvold, T.; Norby, T. *Surf. Interface Anal.* **2000**, *30*, 95.
(13) Iwahara, H. *Solid State Ionics* **1995**, *77*, 289.
(14) Gallini, S.; Hansel, M.; Norby, T.; Colomer, M. T.; Jurado, J. R. *Solid State Ionics* **2003**, *162−163*, 167.
(15) Chen, P.; Mah, T. *J. Mater. Sci.* **1997**, *32*, 3863.
(16) Lucas, S.; Champion, E.; Bregiroux, D.; Bernache-Assollant, D.; Audubert, F. *J. Solid State Chem.* **2004**, *177*, 1302; 1312.

10.1021/cm047945q CCC: $30.25
Published on Web 07/15/2005

tation using $La(NO_3)_3 \cdot 6H_2O$, $Sr(NO_3)_2$, and $(NH_4)_2HPO_4$ as precursors. Monazite phase (monoclinic $LaPO_4$) is directly achieved after drying at 105 °C; however, by TEM analysis the rhabdophane phase (needle-shape crystals) is detected, which can be due to a possible hydration of the monazite phase. Using this synthesis method, NH_4NO_3 and HNO_3 acid are obtained as byproducts and are totally eliminated after calcination at 800 °C. An experiment performed by Arul Dhas et al.[18] describes the preparation of crystalline lanthanum phosphate powder by flash combustion. This is a complex synthesis method that even requires the preparation of the fuel. The preparation method that is described in the present work shows several advantages if compared to the preparation described by those authors:[18] it is more simple (one step); there is no need to synthesize the fuel and no explosion takes place. Fujishiro et al.[19] prepared $LaPO_4$ particles using the hydrothermal reaction of a La(edta)-chelate precursor and phosphate ions. Although monodispersed spherical and spindle-like monazite-type $LaPO_4$ particles are formed by the hydrothermal reaction at 150 °C, a low relative density (91.6%) after sintering at 1400 °C is attained. Ruigang et al.[20] attained a mixture of both rhabdophane and monazite-type $LaPO_4$ powders using a direct liquid−solid reaction of lanthanum oxide and phosphoric acid. Pure monazite-type $LaPO_4$ was obtained by calcining the precursor powders at a temperature higher than 600 °C. The sintering temperature in that work is 1600 °C, much higher than the one required to sinter the $La_{(1-x)}Sr_{(x)}PO_4$ powders in the present work.

As is well-known in ceramic materials science, the synthesis route plays a key role in the final properties of the ceramics. For this reason, it is necessary to test new preparation methods and to analyze the effect on the powder characteristics, microstructure of the materials, and, therefore, on the physical, chemical, and electrochemical behavior.

In recent years, combustion synthesis as a preparative process to produce homogeneous very fine crystalline, unagglomerated, multicomponent oxide ceramic powders without the intermediate decomposition and/or calcining steps has attracted a good deal of attention.[21−26] The combustion synthesis technique consists of bringing a saturated aqueous solution composed of the desired metal salts and of a suitable organic fuel to the boiling temperature, until the mixture ignites and a self-sustaining and rather fast combustion reaction takes off, resulting in a dry, usually crystalline fine powder. While redox reactions are exothermic in nature and often lead to explosion if not controlled, the combustion of metal nitrates−urea mixtures usually occurs as a self-propagating and nonexplosive exothermic reaction. The large amounts of gases formed can result in the appearance of a flame, which can reach temperatures in excess of 1000 °C.

In this work we aim to define a protocol in order to obtain pure and nanometric powders of $La_{(1-x)}Sr_{(x)}PO_4$ (where $x = 0, 0.025, 0.050$) by means of the combustion synthesis using urea as fuel. To sinter $La_{(1-x)}Sr_{(x)}PO_4$ and to use it as a protonic conductor it is very important to obtain dense, gastight, and pure materials since impurities could diminish their ionic mobility.

Experiments

The combustion synthesis was performed using the following powder precursors (analytical grade): $La(NO_3)_3 \cdot 6\ H_2O$, $Sr(NO_3)_2$ and $(NH_4)_2HPO_4$ purchased from Panreac Química S.A, Barcelona, Spain. As mentioned above, urea was used as a fuel (analytical grade purchased from Aldrich, Germany). The precursors and the fuel were previously mixed in a wide-mouth vitreous silica basin employing a glass bar until a uniform viscous liquid mixture was formed. The basin was then placed on a hot plate and heated to 100 °C for 10 min before the final treatment at 300 °C for 1 h. The reaction takes place in a few minutes, leaving a white foam in the basin. The powder obtained by crushing the foam is white and fine and was easily sieved through a 100 μm sieve. The powders were calcined in air at three different temperatures 200, 400, and 800 °C for 12 h, applying a heating rate of 5 °C/min. The final treatments were calcination at 800 °C/12 h in air in order to increase the powder crystallinity and attrition-milling in ethanol for 3 h using 1 mm diameter zirconia balls (purchased from Tosoh, Japan). A final sieve through 100 μm before compaction was performed. The nitrogen content of the powders at each calcination temperature was determined with a LECO TC-436 nitrogen analyzer, employing the gas fusion method.[27] Chemical analysis of the carbon content of the powders at each calcination temperature was performed using a LECO analyzer, CS-200 model. Differential thermal and thermogravimetric analysis (DTA/TG) in air of the as-prepared powder was carried out on a NETZSCH STA-409 Thermoanalyzer, utilizing alumina as the reference material, in the temperature range of 20−1350 °C with a heating rate of 3 °C/min. Phase identification was performed by X-ray diffraction on a Siemens powder diffractometer D-5000, operating at 50 kV and 30 mA, using Cu Kα radiation and a Ni-filter in the range of $2\theta = 10-80°$. The scanning step was 0.05°, the time/step 1.5 s, and the rotation speed 30 rpm. X-ray patterns were collected on the as-prepared powders and at the three calcination temperatures mentioned above. A longer term and wider range scan was employed to obtain the cell parameters: $2\theta = 10-110°$, time/step = 20 s, using Si as an internal standard. These data allowed us to calculate the cell parameters (software 'Unitcell'). Crystallite sizes were calculated by X-ray line-broadening analysis using the Scherrer equation.[28] The average agglomerate size was measured by means of a particle-size laser analyzer provided by Malvern Instruments, model Mastersizer. BET specific surface area of the powders was determined using a Monosorb Analyzer MS-13 QuantaChrome. Infrared absorption spectra in the 400−4000 cm^{-1} frequency range were obtained employing a Perkin-Elmer FTIR spectrometer 1760X on cold-pressed pellets composed of 0.01 g of the prepared powders and 0.3 g of KBr. Particle morphology was observed by scanning electron microscopy and

(17) Gallini, S.; Jurado, J. R.; Colomer, M. T. Accepted for publication in *J. Eur. Ceram. Soc.*
(18) Arul Dhas, N.; Patil, K. C. *J. Alloys Compd.* **1993**, *202*, 137.
(19) Fujishiro, Y.; Ito, H.; Sato, T.; Okuwaki, A. *J. Alloys Compd.* **1997**, *252*, 103.
(20) Ruigang, W.; Wei, P.; Jian, C.; Minghao, F.; Zhenzh, C.; Yongming, L. *Mater. Chem. Phys.* **2003**, *79*, 30.
(21) Manoharan, S. S.; Patil, K. P. *J. Am. Ceram. Soc.* **1992**, *75*, 1012.
(22) Ravindranathan, P.; Komarnemi, S.; Roy, R. *J. Mater. Sci.* **1993**, *12*, 369.
(23) Zhang, Y.; Strangle, G. C. *J. Mater. Res.* **1994**, *9*, 1997.
(24) Muthuraman, M.; Arul Das, N.; Patil, K. C. *J. Math. Synth. Process* **1996**, *4−2*, 115.
(25) Fumo, D. A.; Morelli, M. R.; Segadães, A. M. *Mater. Res. Bull.* **1996**, *31*, 1243.
(26) Colomer, M. T.; Fumo, D. A.; Jurado, J. R.; Segadães, A. M. *J. Mater. Chem.* **1999**, *9*, 2505.
(27) Thomas, A.; Muller, G. *J. Eur. Ceram. Soc.* **1991**, *8*, 163.
(28) Klug, K. D.; Alexander, L. E. *X-ray diffraction procedures*; Wiley: New York, 1974; pp 618−708.

chemically analyzed by energy dispersive X-ray spectroscopy (SEM-EDS) on both Zeiss DSM 950 and Hitachi S-4700 microscopes. Crystallite size and morphology of the as-prepared powders were also estimated by transmission electron microscopy and chemically analyzed by energy dispersive X-ray spectroscopy (TEM-EDS), using a JEM-2000FX microscope. The shrinkage behavior study was performed using a high-temperature dilatometer (Adamel Lhomargy, DI-24 model) at a heating rate of 2 °C/min up to 1500 °C, on uniaxially and isostatically pressed (200 MPa) disks of 2−3 mm thick and 6 mm in diameter of powder previously calcined at 800 °C/12 h.

Results and Discussion

Combustion Reactions. To prepare $La_{(1-x)}Sr_{(x)}PO_4$, where $x = 0$, 0.025, and 0.050, by the combustion route, using urea as fuel, crystalline $La(NO_3)_3{\cdot}6H_2O$ can be used as a La source (total valencies −15), $Sr(NO_3)_2$ as a Sr source (total valencies −10), and $(NH_4)_2HPO_4$ as a PO_4^{3-} source (total valencies +4). Urea, $CO(NH_2)_2$ (total valencies +6), was used as fuel, as mentioned above. For most purposes urea is the most convenient fuel to be used: it is readily available commercially, it is inexpensive, and it generates the highest temperature, although fuel-rich mixtures might produce prematurely sintered particle agglomerates. It is important to avoid a presintering effect during the combustion reaction which may produce large and hard agglomerates difficult to deagglomerate, disabling the densification of the prepared powders. For this reason, an adequate quantity of urea must be employed in the reaction mixture.

Direct use of the propellant chemistry criterion, with the metal precursor and the PO_4^{3-} anion in a 1:1 molar ratio ($LaPO_4$ case), to determine the urea needed to balance the total oxidizing and reducing valencies in the mixture of oxidizers and fuels, leads to

$$(-15) + 4 + 6n = 0$$

where −15 is the total valence of $La(NO_3)_3{\cdot}6H_2O$, +4 is the total valence of $(NH_4)_2HPO_4$, and + 6 corresponds to the total valency of $CO(NH_2)_2$, as mentioned above. The equation gives $n = 1.83$, which means that 1.83 moles of urea are required for each mole of $La(NO_3)_3{\cdot}6H_2O$ or $(NH_4)_2HPO_4$.

Standard thermodynamic properties of the compounds which might be involved in the combustion process are reported in Table 1.[29,30] The combustion reactions are described in Table 2 together with the $\Delta H°$ found in the literature.[29,30] Furthermore, the combustion reaction of urea, described by eq R1 in Table 2, is exothermic and should provide the energy (heat) needed for the synthesis reaction. Besides, if one takes into account that the reaction takes place in an acid environment (pH ≈ 2), the protonation of urea, described as (R2) in Table 2, is very likely to occur. The individual decomposition reactions of the precursor nitrates, leading to the corresponding oxides ((R6) and (R7), respectively), are also listed in Table 2 and the decomposition of $(NH_4)_2HPO_4$ to H_3PO_4 is described by eq (R8). The rest of the equations in Table 2 represent other reactions which also might take place during the combustion synthesis. For instance, (R9), (R10), and (R11) equations describe the possible reaction of each precursor with urea.

Table 1. Standard Thermodynamic Properties of the Compounds Which Might Be Involved in the Combustion Process

compound	$\Delta H_f°$ [kJ mol^{-1}]	$C_p°$ [J mol^{-1} K^{-1}]
$LaPO_4$	−1949	100.950
$(NH_4)_2HPO_4$	−1566.9	188.0
$Sr(NO_3)_2$	−978.2	149.9
$La(NO_3)_3{\cdot}6H_2O$	−3060.7	-
$CO(NH_2)_2$	−318.8	89.04
H_3PO_4	−1284.4	106.1
SrO	−592.04	45.4
La_2O_3	−1793.7	108.68
NH_4NO_3	−365.65	139.12
NH_3	−45.898	35.652
CO_2	−393.133	$43.22 + 0.01145T^a$
H_2O	−241.587	$30.10 + 0.01505T^a$
N_2	0	$27.17 + 0.00418T^a$
O_2	0	$24.74 + 0.01505T^{a,b}$

[a] T is the absolute temperature. [b] Calculated from discrete values.

By X-ray diffraction a single phase was identified as $LaPO_4$ for the as-prepared powder with $x = 0$ (Figure 2). This result suggests that the overall reaction can be described as (R19) equation (Table 2), where $Sr(NO_3)_2$ is included as a precursor.

The fact that the combustion process is not complete, in the sense that no flame is produced, can be due to the low enthalpy of the reaction, i.e., the energy released is not enough to produce a complete combustion. The possible protonation of urea, described as (R2) in Table 2, could be another reason to explain the lack of a flame since the available unprotonated urea in the combustion reaction media might be less than the required amount. Furthermore, as is well-known, urea suffers a thermal decomposition which involves the formation of different compounds (see reactions (R3), (R4), and (R5) in Table 2).[31] This thermal decomposition provokes a depletion of fuel in the reagent mixture. As a consequence, the direct reaction between urea and the rest of the reagents is forced to happen according to a modified stoichiometry.[31,32] In the experiments described in this work, a stoichiometric amount of urea and an excess of 25 mole % were used in order to clarify the reason for an incomplete combustion process.

A further depletion of urea could take place if part of each precursor of the initial mixture reacts with urea; a lesser amount of the fuel will be free for the total reaction. However, it has to be outlined that the addition of an excess of 25 mole % urea to the stoichiometric amount does not change the result of the reaction in any sense. This could indicate that the low enthalpy of the reaction is the main reason to explain the absence of a flame and that the urea depletion has no significant effect in this system.

Powder Characterization. Nitrogen analysis was performed on the combustion product and on the powders calcined at 400 and 800 °C for 12 h. The nitrogen content was 3.1 wt % in the as-prepared powders, 1.0 wt % in the powders calcined at 400 °C, and no nitrogen was detected in the powders calcined at 800 °C. These data could indicate

(29) *CRC Handbook of Chemistry and Physics*, 84th ed.; Lide, D. R., Ed.; CRC Press: Boca Raton, FL, 2003−2004.
(30) Thiriet, C.; Konings, R. J. M.; Javorský, P.; Magnani, N.; Wastin, F. *J. Chem. Thermodyn.* **2005**, *37*, 131.
(31) Biamino, S.; Badini, C. *J. Eur. Ceram. Soc.* **2004**, *24*, 3021.
(32) Podsiadlo, S. *Thermochim. Acta* **1995**, *256* (2), 375.

Table 2. Equations Describing the Reactions That Might Be Involved in the Combustion Process

reaction		$\Delta H°$ (25 °C) [kJ mol^{-1}]
R1	$CO(NH_2)_{2\,(c)} + 1.5O_{2\,(g)} \rightarrow CO_{2\,(g)} + 2H_2O_{\,(g)} + N_{2\,(g)}$	−557.5
R2	$CO(NH_2)_{2\,(c)} + H_3O^+_{\,(c)} \rightarrow CO(NH_2)(NH_3)^+_{\,(c)} + H_2O_{\,(g)}$	
R3	$CO(NH_2)_{2\,(c)} \rightarrow NH_{3\,(g)} + HCNO$	
R4	$CO(NH_2)_{2\,(c)} + HCNO \rightarrow H_2NCONHCONH_2$	
R5	$HCNO + H_2O_{\,(g)} \rightarrow CO_{2\,(g)} + NH_{3\,(g)}$	
R6	$La(NO_3)_3 \cdot 6H_2O_{\,(c)} \rightarrow 0.5La_2O_{3\,(c)} + 6H_2O_{\,(g)} + 1.5N_{2\,(g)} + 3.75O_{2\,(g)}$	715.2
R7	$Sr(NO_3)_{2\,(c)} \rightarrow SrO_{\,(c)} + N_{2\,(g)} + 2.5O_{2\,(g)}$	386.2
R8	$(NH_4)_2HPO_{4\,(c)} + 3/4O_{2\,(g)} \rightarrow H_3PO_{4\,(c)} + 1/2N_{2\,(g)} + 3/2H_2O_{\,(g)} + NH_{3\,(g)}$	125.8
R9	$2[La(NO_3)_3 \cdot 6H_2O]_{(c)} + CO(NH_2)_{2\,(c)} \rightarrow 5La_2O_{3\,(c)} + CO_{2\,(g)} + 14H_2O_{\,(g)} + 4N_{2\,(g)} + 6O_{2(g)}$	
R10	$Sr(NO_3)_{2\,(c)} + CO(NH_2)_{2\,(c)} \rightarrow SrO_{\,(c)} + CO_{2\,(g)} + 2H_2O_{\,(g)} + 2N_{2\,(g)} + O_{2\,(g)}$	
R11	$(NH_4)_2HPO_{4\,(c)} + CO(NH_2)_{2\,(c)} + O_{2\,(g)} \rightarrow H_3PO_{4\,(c)} + CO_{2\,(g)} + 5H_2O_{\,(g)} + 2N_{2\,(g)}$	
R12	$2La_2O_{3\,(c)} + 3H_3PO_{4\,(c)} \rightarrow 3LaPO_{4\,(c)} + La(OH)_{3\,(c)} + 3H_2O_{\,(g)}$	
R13	$2NH_4^+ + 2NO_3^- \rightarrow 2NH_4NO_{3\,(c)}$	
R14	$(1-s)La_2O_{3\,(c)} + 2H_3PO_{4\,(c)} + (2s)SrO_{\,(c)} + (2s)O_2 \rightarrow 2La_{(1-s)}PO_4{:}\ Sr_{s\,(c)} + La_{(1-s)}PO_4{:}\ Sr_s \cdot xH_2O_{(c)} + 3H_2O_{(g)}$	
R15	$SrO_{\,(c)} + CO_{2\,(g)} \rightarrow SrCO_{3\,(c)}$	
R16	$(1-s)La(NO_3)_3 \cdot 6H_2O_{\,(c)} + (s)SrO_{\,(c)} + H_3PO_{4\,(c)} \rightarrow 2La_{(1-s)}PO_4{:}\ Sr_{s\,(c)} + La_{(1-s)}PO_4{:}\ Sr_s \cdot xH_2O_{\,(c)} + {}^3/_2(5-4s)H_2O_{\,(g)} + {}^3/_2(1-s)\,N_{2\,(g)} + (15-16s)/4O_{2\,(g)}$	
R17	$(1-s)La_2O_{3\,(c)} + (2s)Sr(NO_3)_{2\,(c)} + 2H_3PO_{4\,(c)} \rightarrow 2La_{(1-s)}PO_4{:}\ Sr_{s\,(c)} + La_{(1-s)}PO_4{:}\ Sr_{s\,(c)} \cdot xH_2O + (2s)N_{2\,(g)} + 3H_2O_{\,(g)} + {}^3/_2(1+s)O_{2\,(g)}$	
R18	$(1-s)La(NO_3)_3 \cdot 6H_2O\ (c) + (s)SrO_{\,(c)} + H_3PO_{4\,(c)} \rightarrow 2La_{(1-s)}PO_4{:}\ Sr_{s\,(c)} + La_{(1-s)}PO_4{:}\ Sr_s \cdot xH_2O_{\,(c)} + {}^3/_2(5-4s)H_2O_{\,(g)} + {}^3/_2(1-s)N_{2\,(g)} + (15-16s)/4O_{2\,(g)}$	
R19	$(1-s)La(NO_3)_3 \cdot 6H_2O\ (c) + (s)Sr(NO_3)_{2\,(c)} + CO(NH_2)_{2\,(c)} + H_3PO_{4\,(c)} \rightarrow La_{(1-s)}PO_4{:}\ Sr_{s\,(c)} + La_{(1-s)}PO_4{:}\ Sr_s \cdot xH_2O_{\,(c)} + ((19-12s)/2)H_2O_{\,(g)} + ((4-s)/2)N_2 + ((15-16s)/4) + CO_{2\,(g)} + ((9-6s)/4)O_{2\,(g)}$	

[a] (c) = crystalline, (g) = gas, (l) = liquid.

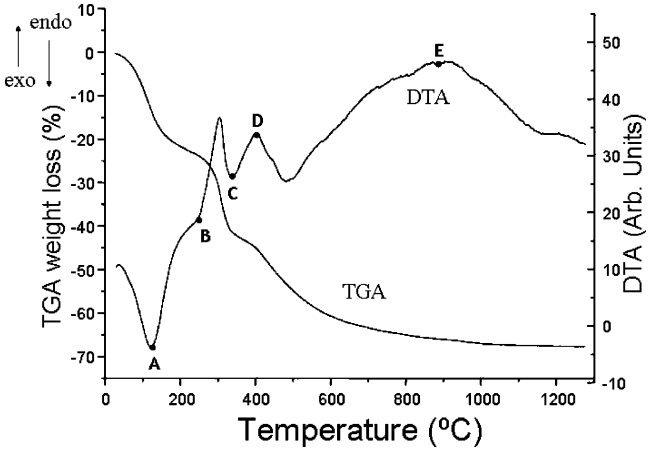

Figure 1. DTA/TG of $LaPO_4$ combustion product.

that the compounds containing nitrogen (NH_4NO_3, NH_3, unreacted nitrate used as precursors, etc.) are retrieved in the as-prepared powders. The carbon content analysis confirms the presence of C in the as-prepared powders (1.0 wt %); however, no carbon is detected in the powders calcined at 800 °C.

TGA data of $LaPO_4$ as-prepared powder (Figure 1) showed a large weight loss (∼68 wt %) between room temperature and 1100 °C. The weight loss could indicate among other phenomena that during the combustion reaction the generated byproducts, such as H_2O, NH_4NO_3, NH_3, etc., have not been completely eliminated. In fact, two endothermic peaks, the first one centered at 120 °C and the second (as a shoulder) at 250 °C (A and B, respectively), are detected in the DTA pattern. The endothermic peak centered at ∼120 °C can be attributed to the loss of physisorbed water, can be also assigned to the orthorhombic to tetragonal (55 °C) and tetragonal to cubic (130 °C) phase transitions, and melting (170 °C) of NH_4NO_3.[33,34] This endothermic peak is accompanied by a weight loss of ∼25 wt%. The second endothermic peak centered at 250 °C (shoulder of the peak centered at 120 °C) could correspond to both the progressive dehydration of the rhabdophane phase and to the decomposition of NH_4NO_3[33,34] (272 °C) and is accompanied also by a loss of weight of about 5%. The water in the rhabdophane crystal is zeolitic water present in its channel-type structure and its dehydration temperature depends on the synthesis method employed.[15,16,19,35−44] On the other hand, as is well-known, the urea undergoes a first decomposition step in the temperature range 154−263 °C; this process happens with a large weight loss, sharp endothermic effect, and vigorous gas emission. Thus, the possible unreacted urea could contribute according to the literature data,[31] to both the weight loss in the TGA and the endothermic process in the DTA in the above mentioned temperature range. A 17% weight loss and a sharp endothermic peak centered at ∼325 °C (C) can be attributed to NO_2 emission. This intermediate compound in the combustion reactions gives rise to the N_2 and O_2 gases.[31] It must be taken into account that in this work the combustion reactions have been written in their final form, with no indication of the intermediate products. Furthermore, different temperature values in the range of 375 to 900 °C are given for the rhabdophane-type $LaPO_4 \cdot nH_2O$ (hexagonal)

(33) Hussain, G.; Rees, G. J. *Propellants, Explosives, Pyrotechnics* **1990**, *15*, 43.
(34) Hussain, G.; Rees, G. J. *Fuel* **1995**, *74*, 273.
(35) Buissette, V.; Moreau, M.; Gacoin, T.; Boilot, J−P.; Chane-Ching, J−Y.; Le Mercier, T. *Chem. Mater.* **2004**, *16*, 3767.
(36) Glorieux, B.; Matecki, M.; Fayon, F.; Coutures, J. P.; Palau, S.; Douy, A.; Peraudeay, G. *J. Nucl. Mater.* **2004**, *326*, 156.
(37) Onoda, H.; Nariai, H.; Maki, H.; Motooka, I. *Mater. Chem. Phys.* **2002**, *73*, 19.
(38) Nishihama, S.; Hirai, T.; Komasawa, I. *J. Mater. Chem.* **2002**, *12*, 1053.
(39) Boakye, E.; Hay, R. S.; Petry, M. D. *J. Am. Ceram. Soc.* **1999**, *82*, 2321.
(40) Jonasson, R. G.; Vance, E. R. *Thermochem. Acta* **1986**, *108*, 65.
(41) Hikichi, Y.; Hukuo, K.; Shiokawa, J. *Bull. Chem. Soc. Jpn.* **1978**, *51*, 3645.
(42) Guo, Y.; Woznicki, P.; Barkatt, A.; Saad, E. E.; Talmy, I. G. *J. Mater. Res.* **1996**, *11*, 3, 639.
(43) Terra, O.; Clavier, N.; Dacheux, N.; Podor, R. *New J. Chem.* **2003**, *27*, 957.
(44) Rajesh, K.; Sivakumar, B.; Krishna Pillai, B.; Mukundan, P.; Warrier, K. G. K.; Nair, V. R. *Mater. Lett.* **2004**, *58*, 1687.

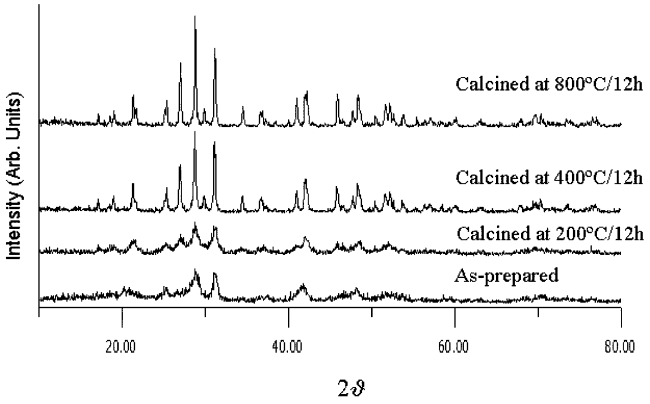

Figure 2. XRD data of $LaPO_4$ combustion product and the same powder calcined at three different temperatures.

to monazite-type $LaPO_4$ (monoclinic) phase transition, according to the revised literature.[15,16,19,35−44] In this study, the exothermic peak at ∼400 °C (D) can be assigned to this transformation. A broad exothermic peak from 500 °C and centered at ∼900 °C (E) is observed and could correspond to both the crystallization of the monazite phase and to the decomposition of organic material. Similar DTA/TG and nitrogen and carbon analysis results are obtained for the Sr-doped compositions.

X-ray analysis data are shown in Figure 2. The data of the as-prepared powder and powder calcined at 200 °C, a temperature below the one reached during the combustion, present low crystallinity; i.e., the peaks are very broad, indicating a small crystal domain. According to the literature,[45] lanthanide orthophosphates exist in five polymorphic forms: rhabdophane, weinschenkite, monazite, xenotime, and orthorhombic symmetries. The X-ray patterns of the as-prepared and dried powders correspond to the rhabdophane-type $LaPO_4 \cdot nH_2O$ (PDF file 46-1439). At 200 °C, the crystallinity increases although the peaks are still very broad. At 400 °C, the X-ray pattern corresponds to the monazite-type $LaPO_4$ (PDF file 32-0493). The monazite crystallinity is improved through a calcination at 800 °C/12 h. As mentioned earlier, by DTA/TG, further crystallization of the monazite phase is developed from 500 to ∼900 °C (exothermic peak).

X-ray data of Sr-subtituted $LaPO_4$ powders were also collected, and no significant variation was found compared to those of pure $LaPO_4$ powder. This can be explained by considering that the monazite structure appears to be an especially accommodating structure since it can accept ions with variable charges and variable ionic radii.[46] In this case, the effective ionic radii of Sr^{2+} and La^{3+} ions are 1.26 Å (Sr^{2+}, coordination number = 8) and 1.18 Å (La^{3+}, coordination number = 8), respectively.[47] The "softness" of the monazite structure may explain the complex chemical composition of natural monazites. The analysis of longer term scans using the "unitcell" software to calculate the cell parameters gave results that confirmed this behavior. From the X-ray diffraction patterns of $LaPO_4$ powders calcined at

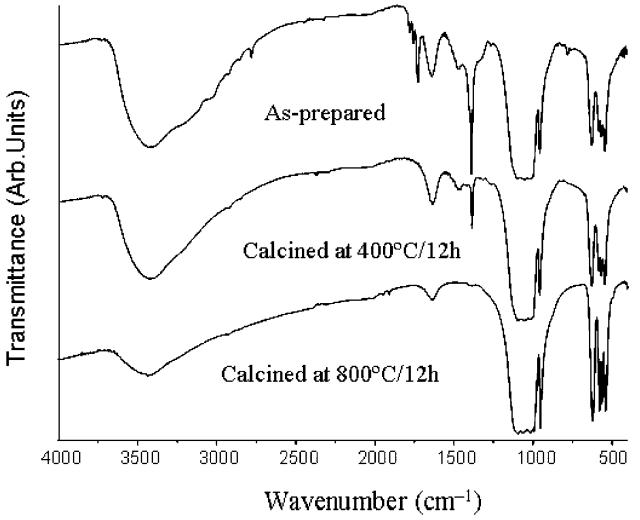

Figure 3. FTIR spectra of $LaPO_4$ as-prepared powder and calcined at two different temperatures, 400 and 800 °C.

800 °C for 12 h, the lattice parameters (monoclinic structure) were calculated and found to be in good agreement with the published data,[35,43,46,48] namely, $a = 0.6847 \pm 0.0003$ nm, $b = 0.7079 \pm 0.0003$ nm, $c = 0.6510 \pm 0.0003$ nm, $\beta = 103.32 \pm 0.09°$, and volume $= 0.3071 \pm 0.0005$ nm^3. The lattice parameters and the lattice volume of $La_{(1-x)}Sr_{(x)}PO_4$ with $x = 0.025$ and 0.050 did not show any significant variation with respect to pure $LaPO_4$.

XRD data were also used to calculate the average crystallite size of the powder calcined at 800 °C: ∼60 nm. This value seems to be confirmed by the TEM analysis (Figure 7). As can be seen, the crystallite size is uniform and is in the 50−100 nm range.

Figure 3 indicates the transmittance bands of the as-prepared $LaPO_4$ powder and the same powder after calcination at 400 and 800 °C/12 h. The band at 1620 cm^{-1} on the FTIR spectrum of the as-prepared powder can be assigned to the hydration water of the hexagonal $LaPO_4 \cdot nH_2O$.[16] This band completely disappears at 400 °C. This indicates that the rhabdophane phase is not present in the powder at this temperature in accordance with the XRD data. The other bands present on the FTIR spectrum of the as-prepared powder are assigned to the phosphate groups. Four bands located at 541, 564, 579 and 617 cm^{-1}, were clearly observed in the υ_4 region of vibration of PO_4 groups.[49,50] The presence of these four bands is characteristic of the vibrations of phosphate groups in the monoclinic structure of monazite-type $LaPO_4$. For the rhabdophane phase there are only three bands in the υ_4 region (541, 579 and 617 cm^{-1}).[16] This fact indicates that the as-prepared powder is a mixture of both rhabdophane and monazite phases, although the XRD does not reveal the presence of the monazite phases. At low frequencies, the five characteristic bands (υ_3 region:

(45) Mooney, R. C. L. *Acta Crystallogr.* **1950**, *3*, 337.
(46) Montel, J.-M.; Devidal, J.-L.; Avignant, D. *Chem. Geol.* **2002**, *191*, 89.
(47) Shannon, R. D. *Acta Crystallogr.* **1976**, *A32*, 751.
(48) Ni, R. C. L.; Hugues, J. M.; Mariano, A. N. *Am. Mineral.* **1995**, *80*, 21.
(49) Farmer, V. C. *The infrared spectra of minerals*; Farmer, V. C., Ed.; Mineralogic Society: London, 1974.
(50) Mullica, D. F.; Milligan, W. O.; Grossie, D. W.; Boatner, L. A. *Inorg. Chim. Acta* **1984**, *95*, 231. Pretsch, E., Clerc, T., Seibl, J., Simon, W. Tablas para la Elucidación Estructural de Compuestos Orgánicos por Métodos Espectroscópicos, Vol. I, Alhambra, Madrid, 1988.

1093, 1060, 1024, 993 and 954 cm^{-1}) of rare-earth phosphates in the monoclinic structure of monazite-type $LaPO_4$, resulting from the distortion of the tetrahedral phosphate groups in the 9-fold coordinated La atoms, can be clearly observed for the calcined powder at 800 °C. The resolution of the vibration bands of phosphate in the domain 990−110 cm^{-1} (υ_3 region) of the FTIR spectra is increased when increases the calcination temperature increases indicating a higher crystallization of the monoclinic phase. Several extra bands are present in the noncalcined powder data and are not present in the powders calcined at 800 °C. IR analysis of the precursors were performed in order to understand the presence of these extra bands. For instance, two bands can be observed in the as-prepared powder spectrum at 1375 and 1470 cm^{-1} that can be associated with both the NO_3^- group of the residual unreacted nitrate precursors and from the NH_4NO_3 formed during the combustion reaction. The experimental IR spectrum of $La(NO_3)_3 \cdot 6H_2O$ shows one band centered at 1385 cm^{-1} and another one at 1468 cm^{-1}; both values match the IR frequencies of the extra bands. In fact, both wavelengths are characteristics of the N−O bond in the NO_3^- group in nitrates. The band at 1468 cm^{-1} could also be assigned to N−H vibrations (1400−1460 cm^{-1}) resulting from the presence of ammonium residues[16] or/and the presence of the biuret ($H_2NCONHCONH_2$) decomposition product of the urea. Another band detected in the as-prepared powders is centered at 1780 cm^{-1} and could be assigned to the N═O bond of the nitrates (unreacted precursors) and from the NH_4NO_3 formed. At 1720 cm^{-1} a band appears that can be associated with the carbonyl group of the unreacted urea or/and the biuret.[50] This band disappears at 400 °C. All these extra bands do not appear in the powders calcined at 800 °C for 12 h. In fact, the carbon content analysis confirms the presence of this element in the noncalcined powders in the amount of 1.0 wt %, as mentioned above, and no presence of carbon is detected for the calcined powders at 800 °C. The bands centered at 1620 and 3500 cm^{-1} can be due to the hydration water (O−H bond) of the rhabdophane phase in the as-prepared powders, as mentioned above, and also to the water adsorbed on the KBr pellet used to perform the IR analysis in the as-prepared and calcined powders. The broad band centered at 3500 cm^{-1} can overlap another one at 3120 cm^{-1} that can be due to the N−H vibration resulting from the presence of ammonium or/and biuret residues[50] present in both the as-prepared and calcined (400 °C) powders, the band being less intense in the latter case. The doped samples show the same bands at every calcination temperature.

The agglomerate average size was studied with a laser analyzer. The data of both the as-prepared and the calcined $LaPO_4$ powder are represented in Figure 4. In all cases, the agglomerate size corresponds to a bimodal distribution. The size range of the as-prepared powder is 0.07−250 μm. There are clearly two peaks in the distribution, one centered at 0.25 μm and the second one at 40 μm. Three differences can be observed in the distribution of the calcined powder at 400 °C with respect to the as-prepared powder: the first one is that the peak at 0.25 μm has a lower intensity, the second is that the peak at 40 μm has a higher intensity than that of the as-prepared powders, and the third one is that the maximum is slightly shifted to a higher value (70 μm) when the powder is calcined. This behavior indicates that the average agglomerate size is increased, a normal phenomenon in polycrystalline materials when they are calcined. To reduce the agglomerate size and to obtain a better sintering behavior, the powders were attrition-milled for 3 h after the final calcination at 800 °C. After the attrition-milling, the agglomerate size distribution is significantly changed: the particle diameter range is 0.15−40 μm and two peaks in the size distribution are still present but they are at different positions from the ones found in the calcined unmilled powders. The new peak positions are at 1 and 20 μm the latter has a very low density and it is clear that the agglomerate size is drastically reduced by about 2 orders of magnitude. Moreover, the agglomerates size was not affected by 2.5% or 5% substitution of Sr in $La_{(1-x)}Sr_{(x)}PO_4$ powders. Attrition-milling for more than 3 h was applied to the powders and no significant differences in either the agglomerates size or their distribution were found.

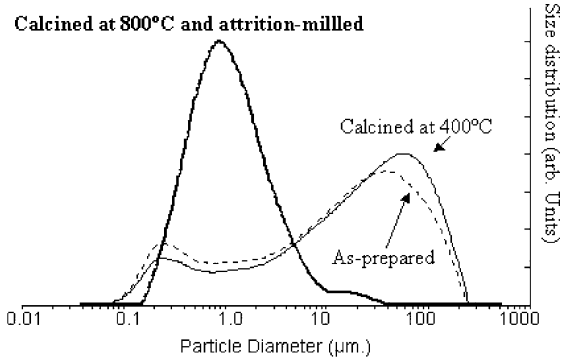

Figure 4. Particle size distribution analysis of $LaPO_4$ as-prepared powder compared to powder calcined at two different temperatures, 400 and 800 °C, and attrition-milled.

SEM micrographs presented in Figure 5 confirm the size range of the agglomerates given by the laser analyzer. Picture 5 (a) shows the as-prepared powder with large agglomerates (some of them larger than 50 μm), picture 5(b) shows a detail of the agglomerates, while the picture on the right side, (5c), corresponds to the calcined (800 °C) and attrition-milled powder where a drastic reduction of the agglomerate size can be observed. Furthermore, the specific surface area of the latter was found to be 7.0 m^2/g, a higher value than that of the unmilled powders. Similar results are observed in the doped powders.

In Figure 6 agglomerates of nanometric crystals of the as-prepared powders can be observed by TEM. The powder exhibits two different morphologies: in some areas needle-like crystals, characteristics of the rhabdophane phase,[17] and in another areas rounded crystals, corresponding to the monazite phase.[17] The electron diffraction of the agglomerates indicates that they are polycrystalline, but the diffraction is not well-defined; in fact, the crystallite size is very small, less than 10 nm. The same technique was used to characterize the powder calcined at 800 °C/12 h. Figure 7 shows round-shaped crystals of $LaPO_4$ powders of a size that varies in the range 40−80 nm. During the heat treatment, the crystals with a needle-like morphology (rhabdophane phase) begin

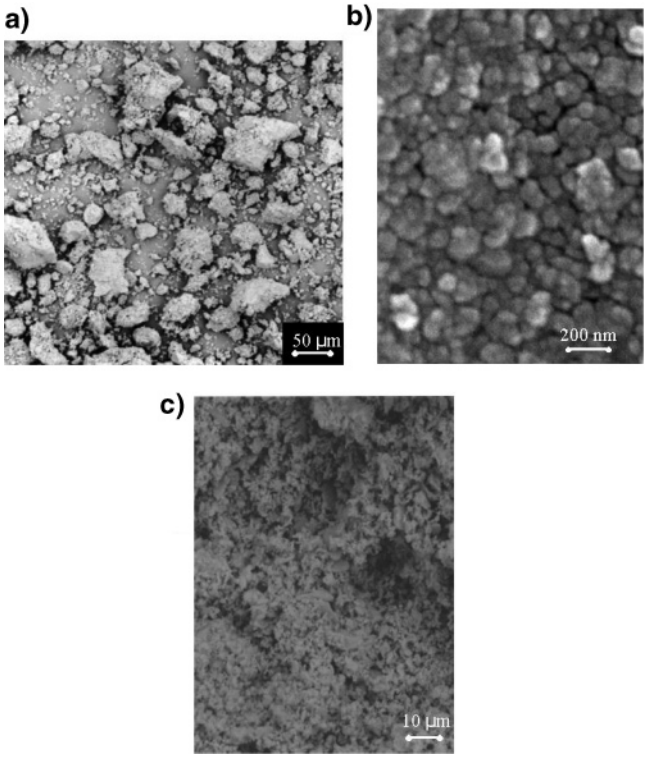

Figure 5. SEM micrographs of as-prepared $LaPO_4$ powder (a) detail of the agglomerates (b) and the same powder calcined at 800 °C and attrition-milled (c).

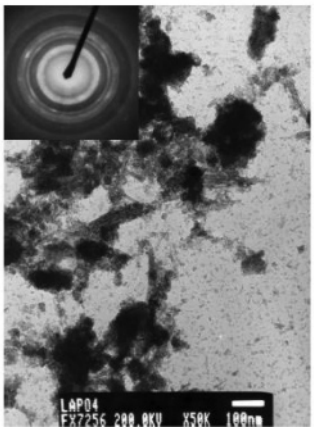

Figure 6. TEM micrograph and electron diffraction pattern of the as-prepared and dried $LaPO_4$ powder.

to change their morphology to an equiaxial shape, characteristic of the monazite phase, due to their transformation. At a calcination temperature of 800 °C, only equiaxial crystals are detected by TEM, corresponding to the monazite phase, as mentioned above (Figure 7). Electron diffraction indicates a good crystallinity; the crystallite size is about 10 times bigger than that in the noncalcined powder.

The last step in the preparation protocol is the attrition-milling for 3 h, as mentioned above. Figure 8 shows how milling affects the size of the agglomerates of nanometric crystals (TEM micrograph). Less agglomerate powder is attained after milling. The crystals are round-shaped as mentioned above, which is a good characteristic in order for packing and to obtain a good sinterability. The doped samples show the same crystal size and morphology than that of the undoped samples. TEM-EDX analysis indicates

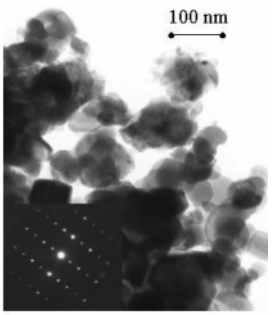

Figure 7. TEM micrograph and a selected area electron diffraction pattern of the $LaPO_4$ powder calcined at 800 °C/12 h.

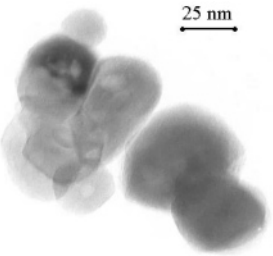

Figure 8. TEM micrograph of $LaPO_4$ powder calcined at 800 °C/12 h and attrition-milled.

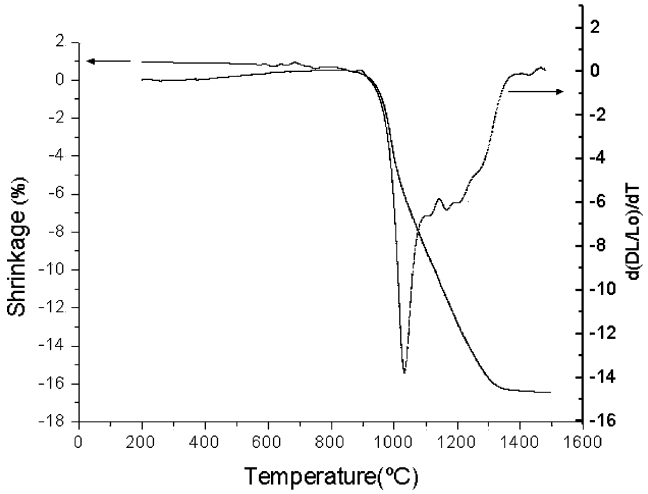

Figure 9. Dilatometric curves, shrinkage vs temperature and shrinkage rate vs temperature of a green pellet of $La_{0.95}Sr_{0.05}PO_4$.

the presence of La, Sr, and P elements in the stoichometric proportions in both as-prepared and calcined powders.

Dilatometric Studies. From the dilatometric curve (Figure 9) of 5% substituted Sr:$LaPO_4$ it can be concluded that the starting densification temperature is ~850 °C and when the temperature increases a large shrinkage (16.5% of the total length) was detected from that temperature up to 1300 °C. The maximum shrinkage rate was achieved at 1030 °C. It is important to outline that the densification behavior is affected by the substitution of La^{3+} by Sr^{2+}. In the case of pure $LaPO_4$, the sintering process is not complete at 1500 °C. However, for the doped samples, the sintering process is complete at ~1300 °C. Thus, Sr^{2+} ions enhanced the densification process, as is expected, since Sr^{2+} generates oxygen vacancies when replaced with La^{3+} ions in the lattice,[9] allowing the sintering temperature to decrease. Therefore, the absence of a flame during the combustion could enhance the densification of the ceramic compacts

because the high temperature, reached when a flame is produced during the reaction, might provoke premature sintering of agglomerates. In addition, for scale-up and industrial production, this synthesis method provides a very rapid and efficient technique for nanometric powders of $La_{(1-x)}Sr_{(x)}PO_4$ compared to other methods.

Conclusions

This work shows that the valency molar proportions of reactants proposed by propellant chemistry can be conveniently used to produce nanometric $La_{(1-x)}Sr_{(x)}PO_4$ powders at low temperature. XRD data reveal that doping with Sr does not affect the volume of the $LaPO_4$ lattice. It has been demonstrated that the homogeneous powders are suitable to obtain dense materials after calcination at 800 °C/12 h and attrition-milling for 3 h. The sintering temperature could be as low as 1300 °C. Unlike other methods, combustion synthesis offers the advantage of simplicity of the experimental setup, a surprisingly short time to obtain the final product and savings in external energy consumption. The fact that the combustion process is not complete in this case can be an advantage because it could enhance densification, which is required for the use of these materials as electrolytes in fuel cells.

Acknowledgments. The authors are grateful to the European RTN project "Investigation of high temperature solid proton conductors of relevance to fuel processing and energy conversion applications" (Contract Number: HPRN-CT-2000-00042) and the Spanish Project MAT2001-1489-CO2-02 for funding.

CM047945Q